

The quantification of anisotropy in graphene/natural rubber nanocomposites: Evaluation of the aspect ratio, concentration, and crosslinking

Bettina Strommer  | Dietmar Schulze | Bernhard Schartel  | Martin Böhning 

Division 7.5 Technical Properties of Polymeric Materials, Bundesanstalt für Materialforschung und -prüfung (BAM), Berlin, Germany

Correspondence

Martin Böhning, Bundesanstalt für Materialforschung und -prüfung (BAM), Unter den Eichen 12205 Berlin, Germany. Email: martin.boehning@bam.de

Abstract

In the processing of nanocomposites, high shear stresses at elevated temperatures orient two-dimensional nanoparticles like graphene. This orientation leads to anisotropic mechanical, thermal or barrier properties of the nanocomposite. This anisotropy is addressed in this study by comparing graphene (few-layer graphene, FLG) with a nanoscaled carbon black (nCB) at a filler content of 3 phr, by varying the vulcanization, and by comparing different FLG contents. Transmission electron microscopy gives insight into the qualitative orientation in the nanocomposite with FLG or nCB. The storage moduli parallel and normal to the orientation reveal the direction dependency of reinforcement through dynamic mechanical analysis (DMA). Dimensional swelling measurements show a restriction of the expansion parallel to the FLG orientation, and an increased expansion normal to the orientation. The vulcanization system and crosslinking determine the respective level of property values, and higher crosslinking densities increase the anisotropy in DMA resulting in values of up to 2.9 for the quantified anisotropy factor. With increasing FLG content, the anisotropy increases. A comparison of the results reveals swelling measurements as the most suitable method for the determination of anisotropy. Compared to recent literature, the presented processing induces higher anisotropy, leading to higher reinforcing effects in the direction of orientation.

KEYWORDS

anisotropy, elastomers, graphene, nanocomposite, orientation, rubber

1 | INTRODUCTION

Incorporating nanoparticles that is, solid particles with at least one dimension smaller than 100 nm,¹ in elastomers is a success story.^{2–7} The reinforcing effect of the nanoparticles in the elastomer matrix is dependent on the type of nanoparticle, the matrix, the concentration and

dispersion of nanoparticles in the matrix, and the interaction between the nanoparticles and the matrix polymer. Depending on the desired nanocomposite behavior, the nanoparticles used are electrically or thermally conductive, stiff, strong, flame retarding, stabilizing, or induce other improvements.^{2,3,8–23} Besides their exceptionally high surface-to-volume ratio, the aspect ratio of the

This is an open access article under the terms of the [Creative Commons Attribution](https://creativecommons.org/licenses/by/4.0/) License, which permits use, distribution and reproduction in any medium, provided the original work is properly cited.

© 2023 The Authors. *Journal of Applied Polymer Science* published by Wiley Periodicals LLC.

nanoparticles plays an important role in their reinforcing ability. For two-dimensional (2D) nanoparticles like graphene (sp^2 -hybridized carbon in hexagonal arrangement, forming sheets of one atom thick layers), the aspect ratio is defined as the lateral-diameter-to-thickness ratio.²⁴ In polymer processing it is widely known that at sufficiently low viscosities at elevated temperatures, shear forces and pressure orient the polymer chains in the material. In the same manner, 2D particles also tend to orient under these conditions when producing polymer nanocomposites.^{25–30} Consequently, the orientation of 2D nanoparticles affects the mechanical properties of the nanocomposites, as reported in the literature. Li et al. determined the spatial orientation of graphene by Raman spectroscopy and calculated the resulting effect on the mechanical properties: compared to randomly oriented nanocomposites, fully aligned graphene yields a Young's modulus increased by a factor of about two for poly(vinyl alcohol) with graphene oxide concentrations of 1–5 wt %.^{31,32} Such an alignment of graphene enables a targeted tailoring of new materials, as the anisotropy within a material may allow the combination of contradictory properties in one material, depending on its direction or orientation.^{32–37}

In elastomers, which are usually rather soft materials, one direction (in-plane, parallel to the orientation of 2D particles) is reinforced, as the nanoparticles produce higher strength; normal to that (cross-plane, normal to the orientation of 2D particles), the material's behavior is dominated by the elastomeric matrix and is therefore soft and damping. The electrical conductivity of graphene results in a conductive elastomer in one direction, and an insulating material in the other direction.^{23,27,38–40} Potts et al. compared the mechanical, thermal and electrical properties of elastomeric nanocomposites prepared via milling (oriented reduced graphene oxide, rGO) or a solution-treated process (weblike network of rGO): The thermal and electrical conductivities were higher in the solution-treated samples, as the direction of electrical or heat “flow” in the measurement setup were normal to the aligned rGO, as determined via transmission electron microscopy.⁴¹ The typical processing steps for elastomeric compounds, roll milling as well as vulcanization and molding in a hot press, are already prone to induce a preferential orientation of the chain molecules constituting the polymeric matrix and of the incorporated (nano-) filler particles. On the other hand, polymeric materials that is, thermoplasts and elastomers, show counteracting relaxation behavior, which also would affect the orientation of individual filler particles. For vulcanized elastomers, the final processing in a hot-press must be taken into account. It is a simultaneous combination of the

shaping process in the compression mold, and therefore the alignment of polymer chains and nanoparticles, with the crosslinking that takes place at the elevated temperature. The simultaneously formed crosslinks might be able to freeze and lock the orientation of both polymer chains and nanoparticles, as the relaxational processes are strongly restricted in vulcanized rubber; see analogous works of Finkelmann et al. on fixing the orientation of elastomeric liquid crystals by crosslinking.^{42–44} Therefore, an influence of the vulcanization system, the obtained crosslinking density, and of the elastomeric matrix is possible.

Our previous studies were focused on the improvements of technical properties,^{8,17,19} potential replacements of conventional fillers by small amounts of graphene^{14,16,18,20} as well as the influence of graphene on the crosslinking kinetics and crosslinking density⁴⁵ in elastomers. In this study, different natural rubber (NR) nanocomposites are evaluated regarding their anisotropic behavior. The influence of the nanoparticle's aspect ratio is addressed using a FLG and a nanoscaled carbon black (nCB) of about the same specific surface area, incorporated into NR and compared to an unfilled reference. Four different vulcanization systems and degrees of crosslinking give insight into the impact of crosslinks on the remaining orientation in the nanocomposites containing FLG. The influence of the 2D nanoparticle content on the anisotropic behavior is evaluated by comparing NR nanocomposites with different FLG concentrations.

The orientation and anisotropic behavior of the rubber nanocomposites are investigated by several methods. First, transmission electron microscopy (TEM) shows FLG and nCB in their dispersed state and arrangement in the nanocomposites. Dynamic mechanical analysis (DMA) in shear mode addresses mechanical properties of small quadrangular rod specimens in two directions. Finally, swelling by immersion of disc-shaped specimens in isoctane as solvent allows the determination of the mass uptake, the overall volume expansion and dimensional swelling in both directions.

The two methods DMA and dimensional swelling allow the calculation of anisotropy factors and a comparison with respect to the reinforcing effect of the nanofillers and the respective anisotropy. These calculations enable the quantification and comparison of the direction-depending property improvements and anisotropy. The presented study aims to investigate important influencing parameters that induce or prevent orientation and anisotropy in elastomeric nanocomposites, and to demonstrate the sensitivities of the methods for their characterization.

2 | EXPERIMENTAL

2.1 | Materials and sample preparation

The comparison with respect to anisotropic reinforcement in this study addresses three aspects: (1) the aspect ratio of the nanofillers, (2) the impact of different cross-linking systems and (3) the influence of concentration of the 2D graphene-related nanofiller. Details and complete recipes for all samples are given in Tables S1 and S2.

As commercially available nanofillers, FLG (available as EXG T 98300 by Graphit Kropfmühl GmbH, Germany) with a BET specific surface area of $326 \text{ m}^2 \text{ g}^{-1}$ and nCB (available as Printex[®] L6 BDS from Orion Engineered Carbons S.A., Luxembourg) with a BET specific surface area of $266 \text{ m}^2 \text{ g}^{-1}$ were used. They were incorporated in natural rubber (NR) via NR latex masterbatch premixing followed by two-roll milling and vulcanization in a hot-press.

For the first comparison (1), two natural rubber composites containing a fixed amount (3 phr) of nanoparticles (denoted NR-FLG and NR-nCB) with different aspect ratios and an unfilled material (NR) were investigated with respect to their effect on swelling and shear modulus in DMA. The nanocomposites containing FLG (NR-FLG) and nCB (NR-nCB) were produced via a masterbatch route using a high-dispersion premixing step for the latex-based solid masterbatch: A 10 g L^{-1} aqueous surfactant solution (cetyltrimethylammonium bromide, CTAB, purchased from AppliChem GmbH, Germany) was prepared in a 5 L beaker and 10 g L^{-1} FLG or nCB were added under stirring. The mixture was dispersed at room temperature (RT) for 1 h using an ultrasonic lance (UPS 400 S ultrasonicator equipped with Horn H22, Hielscher Ultrasonics GmbH, Germany). To maintain the temperature at RT level, the beaker was immersed in a bath of ice water. Diluted NR latex (high ammonia, solid content of 60%, supplied by Weber & Schaefer GmbH & Co. KG, Germany) was added in a calculated amount for a final solid NR-to-nanoparticle ratio of 7:1 in the masterbatch. The dispersion underwent another 3 h of ultrasonication in the described setup. It has to be noted that this mixture containing latex can only be ultrasonicated to disperse the graphene nanofiller when the CTAB surfactant is added. Otherwise, the NR latex would coagulate immediately. To obtain the solid masterbatch, the dispersion was poured into large Petri dishes and left to solidify for 16 h in a ventilating oven at 50°C . Afterwards, the sheets of 1 mm thickness were removed from the Petri dishes, turned upside down and dried for another 48 h at 50°C in the oven. The main processing was conducted on a two-roll mill (Lab Walzwerk MT $6'' \times 13''$, Rubicon Gummitechnik und Maschinenbau GmbH,

Germany) at a temperature set to 50°C , a roll speed of 19 rpm and a friction ratio of 1.1:1 to produce 1 kg of nanocomposite. First, solid matrix NR (TSR-L from Dai Tieng Rubber Corporation, Vietnam) was mixed with the activators zinc oxide (Zinnoxid aktiv from Lanxess Deutschland GmbH, Germany) and stearic acid (BEAROCID SP-1 A from Baerlocher GmbH, Germany), the antioxidant N-isopropyl-N'-phenyl-p-phenylenediamine (IPPD, Vulkanox[®] 4010 NA/LG from Lanxess Deutschland GmbH, Germany), and carbon black (Corax[®] N 660 from Orion Engineered Carbons GmbH, Germany) until a uniform batch was obtained. For NR-FLG and NR-nCB, in a second step the masterbatch was added in an amount to produce nanocomposites with a nanoparticle content of 3 phr and further compounded. Finally, for NR, NR-FLG and NR-nCB, the curatives sulfur (S_8 , with an oil content of 5%, purchased from CS Additive GmbH, Germany) and accelerator di(benzothiazole-2-yl) disulfide (MBTS, Vulkacit[®] DM/CMG from Lanxess Deutschland GmbH, Germany) were incorporated and compounded until mixing was completed (after 30 min in total). Sheets of 2 and 3 mm were pressed and cured at 150°C and 300 bar in a compression mold for 20–24 min, depending on the thickness.

The nanocomposites for the comparison of vulcanization systems (2) and different FLG contents (3) for each of those systems comprise a total of 20 samples. The quantities per sample were reduced for efficiency and mixing was performed in a micro compounder instead of the two-roll mill. The masterbatch was produced in a procedure similar to the previous one, but, as the alkalinity of CTAB greatly affected the vulcanization kinetics, without the surfactant CTAB. The omission of CTAB permits different crosslinkers to be investigated, but necessitated changes in the manufacturing process of the latex-based masterbatch: The aqueous dispersion of 10 g L^{-1} FLG was ultrasonicated for 1 h and diluted NR latex was introduced, part of which coagulated spontaneously. With the addition of 5% formic acid, the remaining NR was coagulated and the final solid masterbatch with a NR:FLG ratio of 2:1 was obtained (50 phr FLG), washed with deionized water until pH neutrality, and dried for 48 h at 50°C to remove excessive water. The main processing, the addition of curatives and the masterbatch in the matrix NR, was conducted in a micro-compounder (MC 15; Xplore Instruments BV, Netherlands) at a temperature of 100°C and a rotational speed of 75 rpm. Four different vulcanization systems were used: two sulfur-based systems with a higher S_8 -to-accelerator system ratio (conventional, SulCon) and a lower S_8 -to-accelerator system ratio (effective, SulEV), and two peroxide-based systems with two different peroxide contents (1 phr peroxide, 1Perox, and 3 phr peroxide, 3Perox). For SulCon and SulEV, the same

activators, zinc oxide, stearic acid, and sulfur were used as described for NR-FLG, NR-nCB and NR. The accelerator system consisted of the two accelerators *n*-cyclohexyl-2-benzothiazolesulfenamide (CZ, available as Vulkacit CZ/EG-C, purchased from Lanxess Deutschland GmbH, Germany) and tetramethylthiuram disulfide (TMTD, available as Dimacit TMTD-PDR-D, purchased from Taminco N.V., Belgium). The peroxide used for 1Perox and 3Perox was a dicumyl peroxide (Perkadox BC-FF) from Akzo Nobel Functional Chemicals B.V, Netherlands. For all nanocomposites SulCon, SulEV, 1Perox and 3Perox, the carbon black used was Corax[®] N 330, obtained from Orion Engineered Carbons GmbH, Germany. For the comparison of the different weight fractions of FLG in the NR nanocomposites, the added amount of masterbatch varied to obtain NR nanocomposites with 0, 1, 3, 5, and 10 phr FLG content in the final, cured samples. For the vulcanization a mold was introduced into the hot-press to form four disc-shaped specimens with a diameter of 36.6 mm and a thickness of 2 mm at a pressure of 300 bar. For the samples with sulfur-based crosslinking the temperature was set to 150°C, for the peroxide-based crosslinked samples to 170°C; the times varied widely depending on the vulcanization systems and the FLG content.

2.2 | Characterization techniques

2.2.1 | Transmission electron microscopy

Transmission electron microscopy (TEM) on cryo microtome sections was conducted with an acceleration voltage of 200 kV using a JEM-2200FS equipped with an in-column Omega-type energy filter from JEOL Ltd., Japan. Zero-loss conventional bright field TEM was implemented with an energy width of 35 eV. The nominally 70 nm thick cryo microtome sections were cut from the samples at -100°C with an Ultracut UCT of Leica, Wetzlar, Germany.

2.2.2 | Dynamic mechanical analysis

Dynamic mechanical analysis (DMA) in sandwich shear mode was conducted on two specimens per measurement, respectively, using a DMA/SDTA861^e, Mettler Toledo, Switzerland. For the temperature program, a frequency of 1 Hz and a strain of 0.01% were set, and the temperature varied from -80 to 40°C at a heating rate of 1 K min⁻¹. The strain-sweep was measured at 25°C and 1 Hz with strain increasing logarithmically from 0.2 to 1000 μm

(0.01%–50%). Each specimen was a quadrangular shaped rod; specimens of NR-FLG, NR-nCB and NR had dimensions of 6 mm × 3 mm × 3 mm, all other nanocomposites of SulCon, SulEV, 1Perox and 3Perox of 10 mm × 2 mm × 2 mm. The assumed alignment direction of the FLG particles is displayed in Figure 1a, with their corresponding surface normal (indicating the plane of the graphene sheets) marked with pink arrows in direction 3. The directions of the microtome cut, of the TEM view and of the force of the hot press applied during processing of the material are also indicated in this scheme.

The directions of the shear load exerted during the DMA measurements are schematically displayed in Figure 1b. Also in this coordinate system, the pressure in the hot-press was applied in direction 3 and the FLG particles would most likely orient in the 1-2-plane. The shear directions of the conducted DMA measurements were parallel to the surface of the pressed plates (γ_{31} , marked with a blue arrow in Figure 1b) and perpendicular to that (γ_{21} , marked with a green arrow in Figure 1b), respectively. Note that the indices of the shear strain γ refer to the surface normal and the direction of strain, respectively. The measurements were conducted on the same specimens, first in parallel and, after a relaxation time of 15 min, in the perpendicular load direction by turning the specimen by 90°. To avoid slippage, the samples had to be compressed by 20% in the sample holder (Figure 1c). This compression load might have an additional influence on the orientation of the FLG; however, there was no other way to measure these elastomeric samples. For comparison the values of the storage modulus G' were taken from the measured G' at 25°C, 1 Hz and 0.1% strain, for all samples and load directions. For an evaluation of the typical error, the samples of 3Perox were measured a second time after 1 week of relaxation. The relative deviation was calculated, and the highest calculated absolute deviation was taken as the error estimate for all DMA results and given in the first line of Table 1.

2.2.3 | Volume and dimensional swelling

Swelling measurements were conducted by immersing three disc-shaped specimens per nanocomposite or reference of a nominal thickness of $h = 2$ mm and diameter $d = 36.6$ mm into isoctane (2,2,4-trimethylpentane, analytical grade, Chemsolute, Th. Geyer GmbH & Co. KG, Germany) at room temperature. Before immersion the specimen discs were weighed (m_0) on an analytical balance with a readability of 0.1 mg, and thickness h_0 and diameter d_0 were determined with readabilities of 0.001

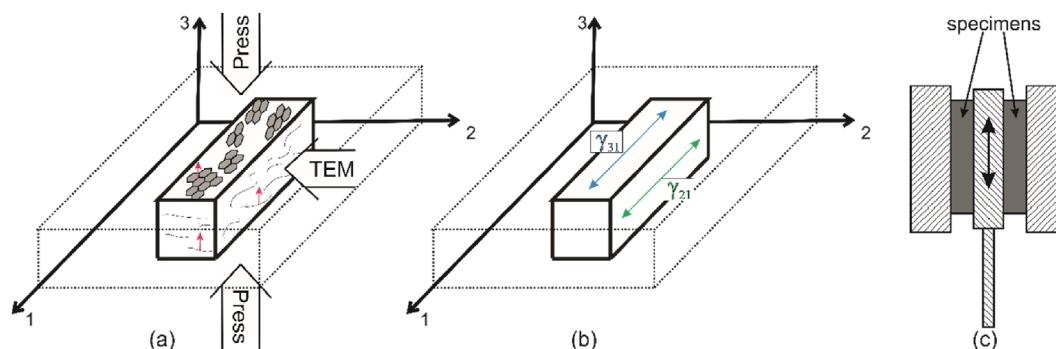


FIGURE 1 Schematic illustration of the shear mode in dynamic mechanical analysis (DMA) measurements in relation to the orientation of the produced nanocomposite sheets (a), the specimen preparation and orientations of applied shear load (b), and in the setup of the DMA in sandwich shear mode (c). [Color figure can be viewed at wileyonlinelibrary.com]

TABLE 1 Results from dynamic mechanical analysis (DMA) measurements from strain-sweep at 0.1% strain, 25°C and 1 Hz and from swelling measurements in isooctane at 23°C.

	FLG content (phr)	$G'(\gamma_{21})$ (MPa \pm 0.03)	$G'(\gamma_{31})$ (MPa \pm 0.02)	$G'(\gamma_{21})/G'(\gamma_{31})$ (\pm 0.1)	h/h_0 (\pm 0.01)	d/d_0 (\pm 0.09)	$(h/h_0 - 1)/(d/d_0 - 1)$ (\pm 0.10)
NR	0	0.43	0.35	1.2	1.5	1.5	1.1
NR-FLG	3	1.2	0.57	2.2	1.5	1.3	1.6
NR-nCB	–	0.65	0.48	1.4	1.5	1.4	1.0
SulCon	0	0.76	0.49	1.6	1.5	1.4	1.1
	1	0.76	0.51	1.5	1.5	1.4	1.3
	3	0.90	0.51	1.8	1.5	1.3	1.4
	5	1.2	0.62	2.0	1.5	1.3	1.6
	10	1.8	0.98	1.9	1.7	1.3	2.2
SulEV	0	0.84	0.38	2.2	1.5	1.4	1.1
	1	0.68	0.37	1.8	1.5	1.4	1.2
	3	1.1	0.56	1.9	1.5	1.4	1.4
	5	1.5	0.66	2.2	1.6	1.4	1.6
	10	2.7	0.96	2.9	1.6	1.3	2.1
1Perox	0	0.32	0.28	1.1	1.6	1.5	1.1
	1	0.36	0.27	1.3	1.6	1.5	1.2
	3	0.43	0.35	1.2	1.6	1.5	1.3
	5	0.51	0.36	1.4	1.6	1.4	1.5
	10	0.70	0.45	1.6	1.6	1.4	1.5
3Perox	0	0.59	0.49	1.2	1.4	1.4	1.1
	1	0.56	0.45	1.3	1.4	1.4	1.2
	3	0.83	0.52	1.6	1.5	1.3	1.4
	5	0.97	0.59	1.6	1.5	1.3	1.5
	10	2.1	1.0	2.0	1.5	1.3	1.8

and 0.5 mm, respectively. After reaching the equilibrium sorption after 49 h, the specimens were removed from the solvent bath, swabbed, and weighed rapidly in a

weighing bottle. Subsequently, diameter d and thickness h of the swollen samples were measured. All measurements were performed at 23°C and 50% rel. humidity.

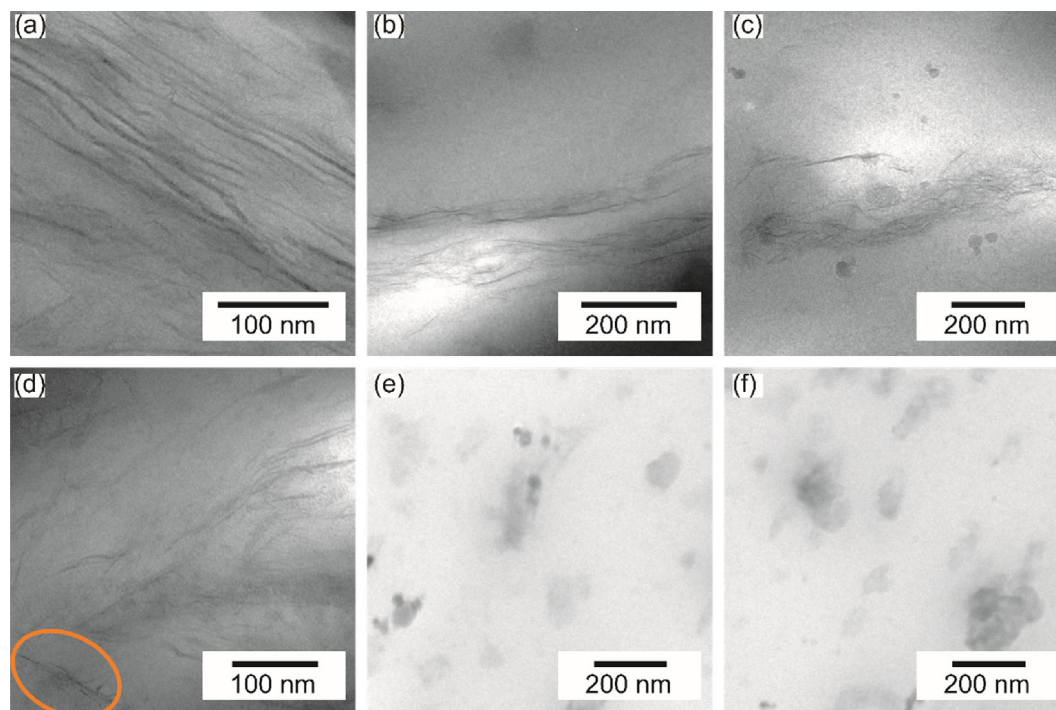


FIGURE 2 Exemplary transmission electron microscopy micrographs of NR-FLG with oriented FLG in (a–d), and of NR-nCB with agglomerated nCB in (e,f). [Color figure can be viewed at [wileyonlinelibrary.com](https://onlinelibrary.wiley.com/doi/10.1002/app.53753)]

3 | RESULTS AND DISCUSSION

3.1 | Transmission electron microscopy

Transmission electron microscopy (TEM) is a useful tool for the characterization of nanocomposites, especially with respect to dispersion, the presence of aggregates or agglomerates, and the spatial distribution of the nanoscale filler particles. High magnifications (600,000X and more) allow the evaluation of the state of dispersion in the surrounding matrix as well as the characterization of the nanoparticles themselves that is, the stack thickness or aspect ratio of FLG. At lower magnifications of 8000 \times or 20,000 \times a larger area of the sample can be inspected in order to reveal possible arrangements or a preferential orientation of the nanoparticles in the matrix. Figures 2a–e show TEM micrographs of NR-FLG, representative for all nanocomposites containing FLG in this study. The microtome sections used for TEM were obtained by cutting the specimens parallel to direction 3 (as defined in Figure 1); the surface normal of the cutting plane was in the direction of coordinate 1 or 2. For better visualization, the direction of the TEM beam is marked in Figure 1. The stacked graphene layers of the FLG particles were therefore nicely visible, as they were oriented parallel to the 1–2 plane, and could be characterized by their thickness (i.e., the typical number of layers). The aspect ratio of FLG, defined as the ratio between the thickness and lateral size of the stacks, was

determined to have a value between 37 and 148; the stack thickness was about 12 atomic layers. Each micrograph indicates the FLG's preferential direction of orientation. As the examined microtome sections of elastomers are not single, uniform films, but several small pieces on one sample carrier, the absolute directions over all micrographs are diverse. The oriented graphene stacks in the different micrographs are not perfectly parallel, but nevertheless show an obvious preferred direction. In the left bottom corner of Figure 2d, marked with an orange ellipse, a counter-directed particle can be seen, but is clearly an exception. Even though there were only few such contrariwise oriented or non-directed particles, they might contribute to the performance of the nanocomposite by connecting the oriented FLG with one another in the direction of thickness.

Figure 2e,f show micrographs of NR-nCB to reveal the structure and shape of nCB. The spherical particles had an aspect ratio of approx. 1 and were arranged in agglomerates without the formation of a continuous network. A formation of such a network was not possible at the low filler content of 3 phr.

3.2 | Dynamic mechanical analysis

Applying an oscillating mechanical load is the principle of dynamic mechanical analysis (DMA). In this study,

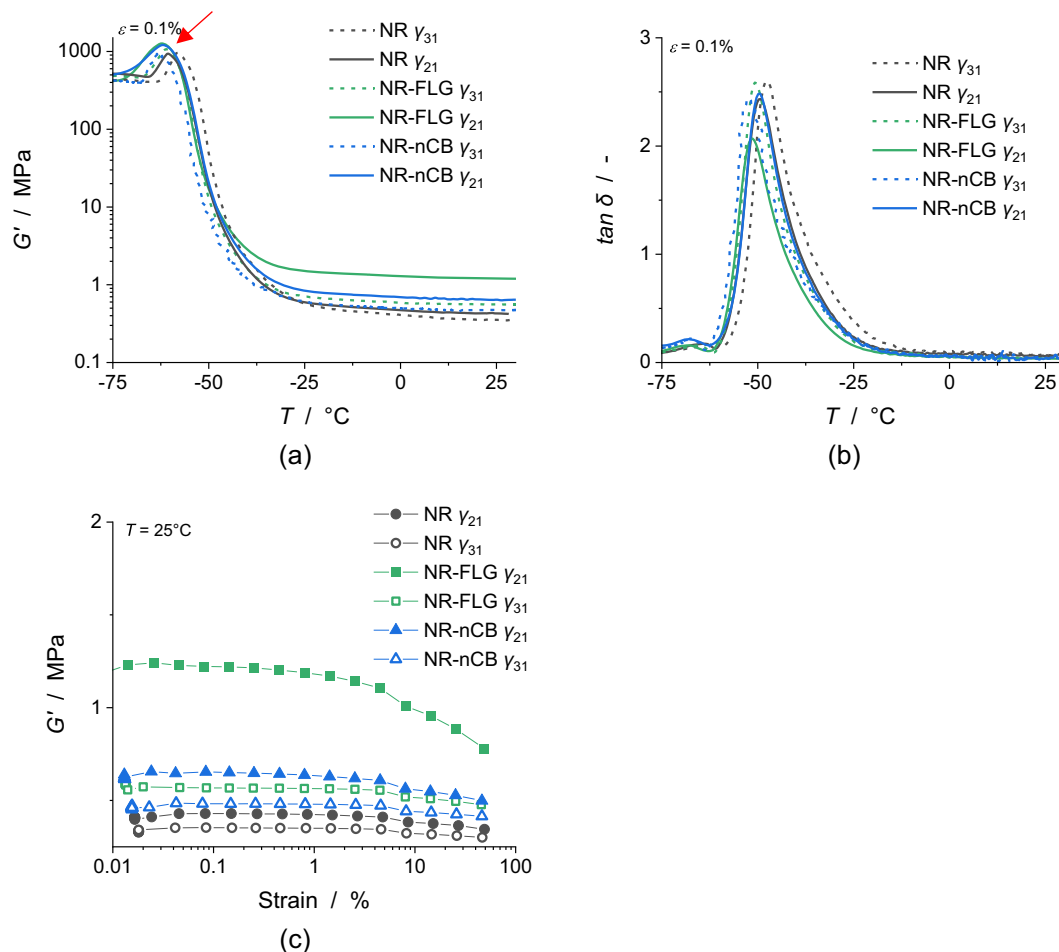


FIGURE 3 Results of dynamic mechanical analysis measurements of NR, NR-FLG and NR-nCB: storage modulus G' over temperature T (a), damping factor $\tan \delta$ over temperature T (b), storage modulus G' over strain (c). For each nanocomposite, NR-FLG and NR-nCB, as well as for the unfilled NR, the curves are shown in parallel load direction (γ_{31}) with dotted lines and open symbols, and in normal load direction (γ_{21}) with compact lines and filled symbols. [Color figure can be viewed at wileyonlinelibrary.com]

sandwich shear mode was used to determine the materials' response to an applied mechanical shear force (at varying temperature or strain), yielding the storage modulus G' and the damping factor $\tan \delta$ (ratio of loss-to-storage modulus G''/G'). The sandwich setup consists of two identical specimens in symmetrical arrangement fixed between two stationary clamps, with one moving element in the middle; see Figure 1c.

The results of the DMA measurements comparing the different filler types of NR-FLG, NR-nCB and NR are visualized in Figure 3, and those of the samples representing the different crosslinking systems of SulCon, SulEV, 1Perox and 3Perox in Figure 4. Both address the anisotropic behavior of the materials by measuring two orientations, respectively, as described in Section 2.2.2.

In Figure 3a the large drop in G' over several orders of magnitude at about -50°C indicates the glass transition temperature (T_g). The increase of G' below the glass transition temperature range (marked with a red arrow)

resulted from the compression applied to the samples to avoid slippage and the resulting stress due to thermal expansion with increasing temperature. The value of T_g differed slightly between the studied samples and orientations, but no clear trend was observed. The damping factor $\tan \delta$ over temperature is shown in Figure 3b, representing the ratio between loss modulus G'' and storage modulus G' . $\tan \delta$ describes how much of the energy applied to the material by the measuring device is dissipated. The peak maximum corresponds to the glass transition, whereas the level of $\tan \delta$ is an indication for the damping behavior of the material. In normal load direction γ_{21} , the maximum values of $\tan \delta$ were in the same range for NR and NR-nCB compared to parallel load direction γ_{31} , whereas FLG in γ_{21} reduced $\tan \delta$ by 25% compared to γ_{31} for NR-FLG.

Figure 3 shows a comparison of FLG and nCB as reinforcing nanoparticles at 3 phr in NR, representing different aspect ratios: the storage modulus G' (Figure 3a) and

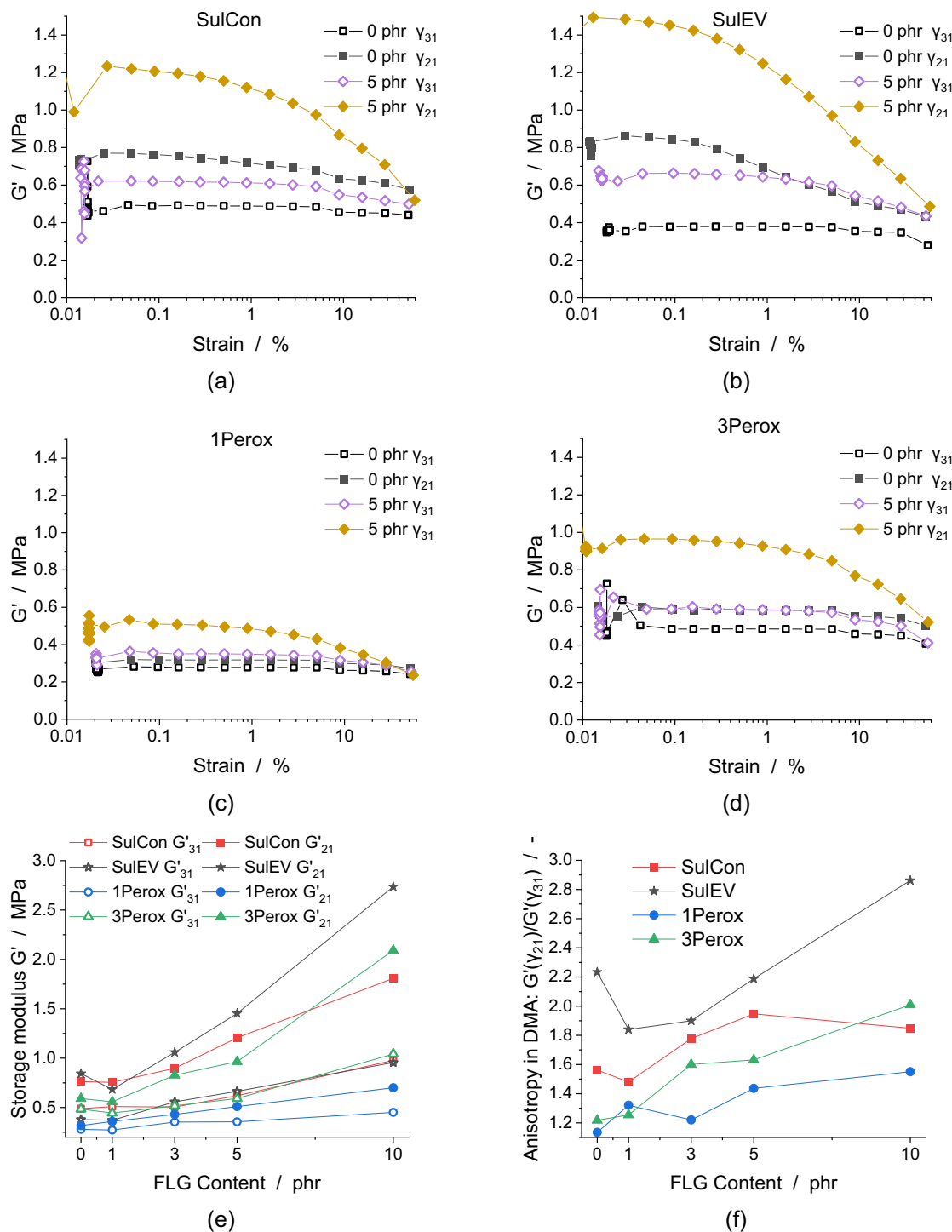


FIGURE 4 Influence of 5 phr few-layer graphene (FLG) on the four studied curing systems, in the parallel load direction γ_{31} (empty icons) and in normal load direction γ_{21} (filled icons), as storage modulus G' at 25°C over logarithmic strain in (a–d). Resulting G' at 0.1% strain in both load directions and anisotropy factor (as the ratio between $G'(\gamma_{21})$ and $G'(\gamma_{31})$) over FLG content in (e) and (f), respectively. [Color figure can be viewed at wileyonlinelibrary.com]

damping factor $\tan \delta$ (Figure 3b) over temperature and G' over strain in Figure 3c. The two load directions result in different absolute values and curve progressions for all three studied samples. This difference indicates anisotropic behavior of all samples, even of the unfilled NR

material. However, this effect is more pronounced for the two nanocomposite systems and becomes dominant for the 2D graphene nanofiller. The anisotropic behavior of the unfilled NR sample indicated an orientation of the molecular polymeric structure. Interestingly, the

spherical nCB as filler also led to a more distinct difference in G' between the two load directions, although these nanoscaled filler particles are assumed to induce an isotropic reinforcing effect. This difference in G' for NR-nCB was related to the process-induced anisotropy, as observed for the unfilled NR. The more pronounced effect in NR-nCB may be related to altered viscosity and relaxation behavior with respect to the process-induced anisotropy. For FLG a strong reinforcing effect was obtained in both load directions, as reflected by significantly higher G' values (Figure 3c). Due to the shape of FLG as a 2D platelet nanoparticle and its orientation and alignment, the difference between normal and parallel load direction was greater than in NR-nCB and NR. The values of $G'(\gamma_{21})$ and $G'(\gamma_{31})$ obtained from the normal and parallel load directions in strain-sweep mode at 0.1% strain, and the derived anisotropy factors as ratios between $G'(\gamma_{21})/G'(\gamma_{31})$ are listed in Table 1. The curve of $G'(\gamma_{21})$ of NR-FLG over strain in Figure 3c showed a decrease in modulus at strains above 1%. This drop in modulus was a result of the breakdown of the filler-filler interaction, according to Payne.⁴⁶

The two DMA methods, temperature-sweep and amplitude-sweep, led to the same values of storage moduli under the same conditions: G' at 25°C and 0.1% strain was the same for both consecutive measurements in the three samples NR, NR-nCB and NR-FLG (linear viscoelastic area). Therefore, the low temperatures or small strains applied in preceding DMA measurements did not change the material behavior. For the following nanocomposites of SulCon, SulEV, 1Perox and 3Perox, the influence of crosslinking was addressed only by conducting and discussing strain-sweep measurements. The respective results of the storage moduli are listed in Table 1, along with the ratio of G' measured in both load directions. The anisotropy factor, calculated by division of $G'(\gamma_{21})/G'(\gamma_{31})$ resulted in a value of 2.2 for the 2D nanoparticle containing NR-FLG, compared to a value of 1.2 for the unfilled NR. To visualize the effect of the 2D nanoparticles FLG, Figure 4a–d show the G' curves over the logarithmic strain for the unfilled NR (0 phr FLG) and 5 phr FLG for SulCon, SulEV, 1Perox and 3Perox, respectively, and in both load directions, normal γ_{21} (filled symbols) and parallel γ_{31} (open symbols) to the expected plane of orientation.

The samples SulEV and 3Perox clearly show the strongest reinforcement of the four vulcanization systems, namely the highest shear modulus G' perpendicular to the plane of the graphene platelets, compared to their unfilled samples with 0 phr; see Table 1 and Figure 4e. For SulEV a first decrease in G' was detected (from 0 to 1 phr FLG), which corresponds to a reported prevention of crosslinking with the presence of FLG.⁴⁵ The values

for 1Perox were lower overall than for the other three vulcanization systems.

The resulting ratio of $G'(\gamma_{21})/G'(\gamma_{31})$ (anisotropy factor) at 0.1% strain enables a quantification of the direction-dependency of the mechanical properties and is plotted over the FLG content in Figure 4f. Similar to the general levels of G' , the anisotropy factors also differ significantly depending on the vulcanization systems. The samples with sulfur-based crosslinker had a distinctively higher anisotropic factor even in the unfilled samples. Upon incorporating FLG, the SulEV system reaches the highest values for reinforcement (represented by G') as well as for the corresponding anisotropy, followed by the SulCon system for crosslinking. The two peroxide crosslinkers yield significantly less reinforcement at similar nanofiller loadings, in combination with less distinct anisotropy as well. Nevertheless, for all nanocomposites containing FLG a more or less pronounced increase in the anisotropy factor was observed with increasing FLG content. When only the two peroxide-based systems and their nanocomposites with different FLG content were compared, 3Perox exhibited higher anisotropy factors than 1Perox. The higher peroxide content in 3Perox is clearly related to a higher crosslinking density in the final elastomer material. Apparently, the higher density of crosslinks enables a stronger fixation of process-induced orientation in the hot-press, whereas a looser network might allow a partial relaxation in the orientation of both the FLG and the polymer chains.

A perfectly isotropic material shows the same mechanical values in all directions and therefore results in an anisotropy factor of 1. All the studied samples had anisotropy factors above 1, which proves that the elastomeric chain themselves are oriented during processing in the first place. Therefore, it is evident that nanoparticle orientation originates from the same cause of deformation and high pressure at elevated temperatures.

3.3 | Swelling

A swelling measurement determines the ability of a material to take-up a solvent. A volume expansion goes hand in hand with the mass increase linked to the solvent uptake. The network structure of the elastomer hinders this process: a rather loose network of covalent crosslinks allows swelling up to a certain degree. A denser network further limits the capacity for volume expansion and therefore also limits the mass uptake of solvents. Consequently, the measurement of the volume increase enables the calculation of a density of crosslinks, according to Flory and Rehner.⁴⁷ Reinforcing fillers in composites act as physical crosslinks forming a network

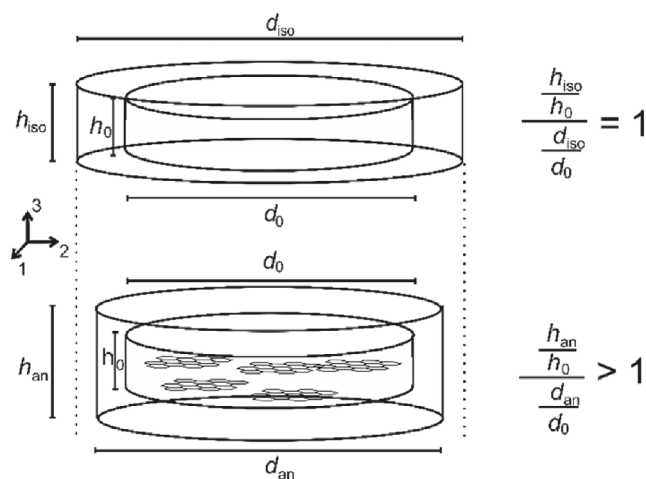


FIGURE 5 Schematic illustration of isotropic (top) and anisotropic (bottom) dimensional swelling.

structure, in addition to the covalently chemical cross-linking network of a vulcanizate. Kraus described the influence on the swelling behavior of such filled elastomers and pointed out the similarity of both networks.^{48–50} To give an overview of the influence of the nanoparticles, the mass sorption over time for NR, NR-FLG and NR-nCB is displayed in Figure S1a; the equilibrium sorption values in mass and volume are given there in Table S3. For an estimation of the sorption kinetics, Figure S1b shows the normalized sorption (normalized to the respective equilibrium sorption level) over the square root of time for NR, NR-FLG and NR-nCB, which reveals only a slight deviation from Fickian behavior and only minor changes in mass uptake rates for all samples. Fickian diffusion kinetics is characterized by a linear increase of the normalized sorption when plotted vs. square root of time. Deviations from this ideal behavior would indicate changes of the local diffusivity due to a significantly altered host matrix caused by the mass uptake of the solvent. An influence on the sorption kinetics of the presence of the nanoparticles or their aspect ratio was therefore not detected. The respective curves of mass uptake over time and kinetics for the vulcanization systems and FLG contents are part of a previous study.⁴⁵

When the polymer chains are oriented or the reinforcing effect of the fillers is more pronounced in one direction than the other, the swelling becomes anisotropic. Furthermore, these two effects may be mutually amplified. As sketched in Figure 5, the different dimensional changes in diameter d and thickness h were used to determine a possible preferential orientation, and the resulting reinforcing effect in these directions in terms of limited expansion. In the disc-shaped specimens the diameter d direction represents the in-plane directions

1 and 2 (see Figure 5) in which 2D nanoparticles are likely to be oriented, and normal to that, the thickness h in direction 3.

For the two different nanofillers and the unfilled NR, Figure 6a shows the increased linear dimensions d and h , and the overall volume V in percent compared to dimensions and volume before immersion in the solvent, d_0 , h_0 , and V_0 , respectively. Table 1 gives the relative dimensional swellings d/d_0 and h/h_0 , as well as the calculated anisotropic swelling (anisotropy factor).

The aspect ratio of the nanoparticles in a nanocomposite affects the anisotropic swelling distinctly, as can be seen in Figure 6a. The incorporation of nCB slightly reduced both d/d_0 (red bars) and h/h_0 , (green bars) compared to unfilled NR. This almost isotropic change reflects the increase of physical crosslinks due to interaction between the polymer matrix and rigid filler particles. In contrast, FLG even led to an increased h/h_0 in combination with a significantly decreased d/d_0 , showing the limited swelling in the graphene plane direction. The quantified swelling anisotropy in form of the anisotropic factor results in 1.61 for NR-FLG, compared to 1.08 for the unfilled NR. This anisotropy in the swelling is similar to the reinforcing effect indicated by $G'(\gamma_{21})$ in the DMA measurements. This direction-dependency underlines the detected preferential orientation of the 2D platelets of FLG. The overall reduction in volume expansion as well as in mass uptake is much more pronounced for FLG than for nCB.

Figures 6b–e show the dimensional and volume increase after swelling as a function of FLG content for NR nanocomposites crosslinked with SulCon, SulEV, 1Perox and 3Perox, respectively. Even though the general level of swelling in both dimensions and the volume were mainly determined by the vulcanization system, clear trends were observed: with increasing FLG content, the increase in diameter d/d_0 (red data points) was reduced, whereas the thickness increase h/h_0 actually rose (green data points). The ratio between $(d/d_0 - 1)$ and $(h/h_0 - 1)$, defined as anisotropic swelling to quantify the anisotropy by Liu et al., over FLG content is shown in Figure 6f for all vulcanization systems and shows similar trends.²⁸ Interestingly, both sulfur-based crosslinkers result in linear behavior for all FLG contents up to 10 phr, resulting in anisotropy factors above 2, whereas the two peroxide systems show negative deviations at the highest FLG concentrations.

The volume expansions clearly decreased with increasing FLG content up to 3 phr FLG for all studied nanocomposites. With a further increase in FLG content in 5 and 10 phr FLG, the V/V_0 of the sulfur-based nanocomposites increased again. This increase in volume expansion results from a simultaneous increase in h/h_0

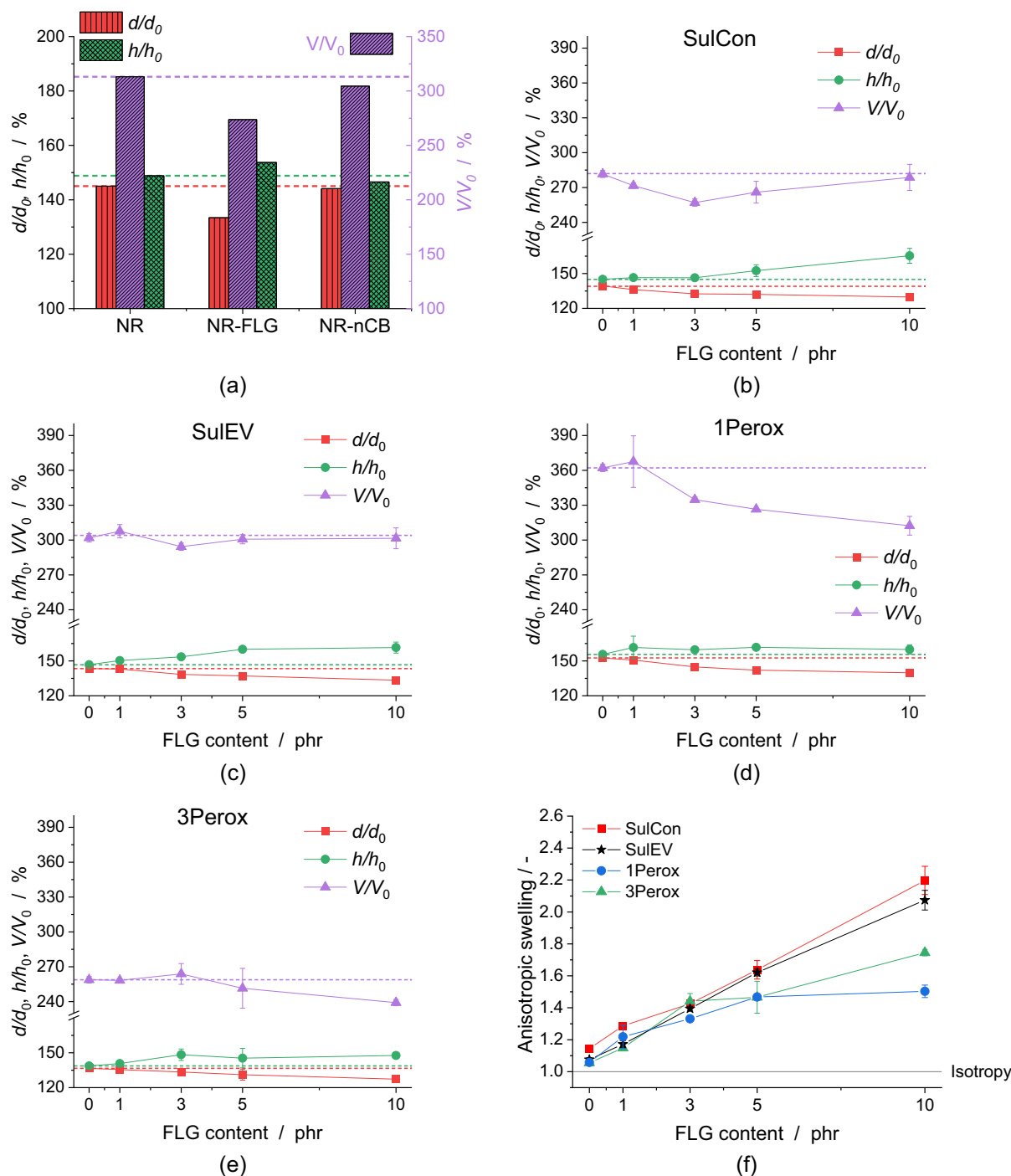


FIGURE 6 Results of volume and dimensional swelling measurements of disc-shaped specimens in isoctane at 23°C; dotted references set on the levels of the unfilled samples (natural rubber and 0 phr few-layer graphene). [Color figure can be viewed at [wileyonlinelibrary.com](https://onlinelibrary.wiley.com/terms-and-conditions)]

and decrease in d/d_0 in SulCon and SulEV, whereas the thickness expansion h/h_0 remained constant between 3 and 10 phr for the peroxide crosslinked nanocomposites. The increase in h/h_0 compared to the lower filled and unfilled samples indicated a sort of reduced reinforcement of the material in this direction, allowing a

more pronounced expansion in thickness. This difference between the nanocomposites of sulfur- and peroxide-based vulcanization was mirrored in the anisotropic swelling for the higher FLG contents, with SulCon and SulEV yielding higher anisotropy factors values than 1Perox and 3Perox.

3.4 | Comparison of the reinforcement and the anisotropy factors

The presented methods allow the calculation of anisotropy factors. In the data obtained from DMA, the anisotropy factor describes the ratio of storage moduli between the normal and parallel load direction in the supposed orientation. Agnelli et al. studied NR nanocomposite in a DMA setup similar to the one presented in this study. The determined anisotropy indices were lower for the nanoscaled graphite they studied in natural rubber at a similar load level of 4 phr. This might result from a different aspect ratio of the nanoparticle compared to the FLG in this study. The incorporation of CNT led to higher anisotropy, and different carbon black types resulted in almost isotropic behavior.²⁶ From the dimensional swelling in a solvent, another anisotropy factor can be obtained, namely as the ratio between thickness increase and diameter increase. Comparing the results from the nanocomposites in this study with the recent literature, our specimens containing FLG yielded higher anisotropy factors in swelling. Liu et al., using graphene nanoplatelets at a content of 5 phr in NR, reported lower ratios between the thickness increase h/h_0 and the diameter increase d/d_0 .²⁸ The differences in DMA and swelling results compared to the recent literature probably arise from small differences in the setups (i.e., choice of solvent, sample sizes, etc.), the processing and the 2D carbon particle studied, as the various manufacturing processes can affect their performance as reinforcing filler. Therefore, in the first place the levels of the obtained values characterizing anisotropy in form of shear moduli in DMA and dimensional swelling may vary, depending on the details concerning material and measurement of the respective study. The reached equilibrium swelling level strongly depends on the vulcanization system even though oriented 2D nanoparticles change the relative values. The anisotropy factors calculated from these methods are also sensitive to these differences and a direct comparison needs caution. Additionally, the conventional processing of the nanocomposites for this study with latex premixing followed by two-roll milling and hot-pressing brings a difference to the recent literature, as the orientation of the FLG is introduced as a side effect in these processing steps and no extra orientation procedure is applied.

The quality of dispersion and distribution of the graphene species in the NR matrix is expected to play a major influencing role, which is realized via an ultrasonic assisted latex masterbatch route in the present study. This premixing step most likely affects predominantly the initial distributive mixing as well as the dispersion (separation of the agglomerates) without a further distinct

exfoliation of the FLG particles (reduction of the number of monoatomic layers in a single graphene stack). The resulting values of $G'(\gamma_{21})$ and anisotropy for NR-FLG were higher compared to all other samples containing FLG, especially the sample with 3 phr FLG content. This difference is presumably because NR-FLG was produced via the combination of two-roll milling and hot-pressing, whereas all other nanocomposites containing FLG were compounded in the microcompounder, followed by hot-pressing. Apart from the higher dispersion, due to the strong influence of ultrasonication and surfactant on reinforcement,¹⁹ the two-roll mill produced a sheet, which was then transferred directly to the hot-press, whereas the product of the microcompounder consisted of crumbs that were randomly placed into the mold for hot-pressing. The two-roll mill and hot-press therefore produced an orientation in the same direction in the 1–2 plane shown in Figure 1a, which was impossible with the compound obtained from the microcompounder. However, all samples of SulCon, SulEV, 1Perox and 3Perox showed anisotropic behavior in the DMA, pointing out the importance of hot-pressing on the orientation of the nanoparticles and polymer chains.

In Figure 7a shows the relation between the $G'(\gamma_{21})$ and the anisotropy factor obtained from DMA. A trend of increasing reinforcement, namely in the $G'(\gamma_{21})$, was observable for the samples, yielding a distinct orientation of the fillers and anisotropic behavior. This result underlines the importance of identifying anisotropy and quantifying it. Only the knowledge about the presence and amount of orientation in a nanocomposite allows the full reinforcing effect of graphene and its derivatives to be exploited in elastomeric matrices.

When the two anisotropy factors obtained in this study for the same samples from DMA and swelling are brought into relation, they roughly correlate, see Figure 7b. However, there are some outlier results, so that a linear regression results in a R^2 of only 0.43 and may be considered as more of a guideline. The DMA results from SulCon and SulEV, especially, differ strongly from the results from swelling, and the unfilled samples yielded rather high anisotropy factors in their storage moduli. The results demonstrate that the method of dimensional swelling measurement results in more predictable values for the anisotropy factor that is, higher anisotropy factors for samples containing 2D nanoparticles. The swelling measurement is easy to set up and is a standard method in elastomer research and industry to determine the crosslinking density by the gravimetric solvent uptake. The small addition to this method of measuring the increase in two dimensions gives reliable insight into the anisotropic behavior of nanocomposites, but also of elastomeric materials in general.

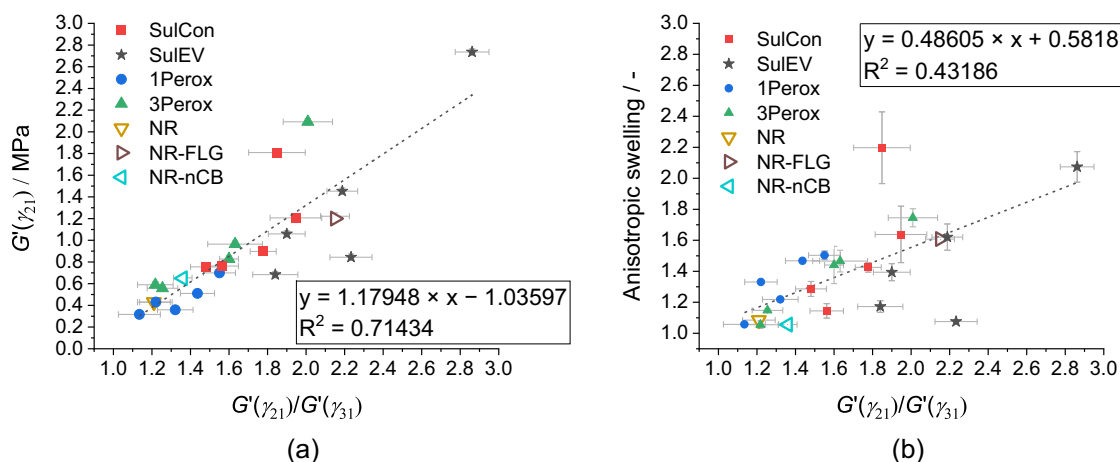


FIGURE 7 Correlation between $G'(\gamma_{21})$ and the anisotropy factor from dynamic mechanical analysis (DMA) (a), and the anisotropy factors from swelling and DMA (b). [Color figure can be viewed at wileyonlinelibrary.com]

The crosslinking system and the resulting crosslinking density affected the anisotropy factors obtained from DMA results more than the anisotropy factors from swelling. For the FLG contents of 0, 1, 3, and 5 phr, the anisotropy in swelling was almost independent of the crosslinking system. At 10 phr some differences were detected, with the nanocomposites obtained via peroxide-based vulcanization exhibiting lower levels than the sulfur-based vulcanizates. However, for the peroxide nanocomposites, the trends of results from DMA correspond with the swelling results.

Without a doubt, the knowledge of a potential preferential orientation of the filler particles and the extend of such is necessary to assess an increased modulus, mechanical strength and other technical properties, especially since the conventional processing techniques implement these orientations in the first place without purpose. Less preferential orientation results in a lower reinforcing effect in the respective direction, but on the other hand a higher reinforcement in the other directions. For applications requiring an isotropic material, such orientations are maybe not desirable—however the FLG increases the storage modulus in the direction normal to the orientation, too, compared to unfilled NR. Therefore, even if the FLG is randomly distributed in the elastomeric matrix, an improvement of mechanical properties is expected. To fulfill its full potential, however, the exploitation of the anisotropy due to an implemented orientation is favored.

4 | CONCLUSION

Two-dimensional nanoparticles can orient or align in the case of the processing of elastomeric nanocomposites due

to shear forces and pressure at elevated temperatures. This orientation influences the properties in different directions, leading to anisotropic behavior. The presented work studies the anisotropy of natural rubber nanocomposites with FLG by transmission electron microscopy, DMA, and dimensional swelling. In comparison to nCB, the incorporation of FLG significantly increases anisotropy by factors of 2.2 (DMA) and 1.6 (swelling) at a filler content of 3 phr. However, minor anisotropy is even observed in unfilled NR, indicating that the processing induces a slight orientation and alignment of the polymer chain molecules. The influence of different vulcanization systems and degrees of crosslinking is generally less on swelling than on the mechanical behavior, as revealed by DMA in shear mode. The investigation of incorporating similar nanoparticles into NR matrices with different crosslinking systems shows their distinct impact on the resulting properties of the nanocomposites. While there is a direct influence of the nanoparticles on the actual crosslinking reaction,⁴⁵ the major effects on the final orientation and alignment of the nanofiller might be the viscosity and relaxation behavior during the processing period.

Two-dimensional swelling measurements generally provide more reliable quantifying results than DMA. Micrographs obtained via TEM are meaningful qualifying tools for characterizing nanocomposites with 2D fillers and detecting a preferential orientation. In contrast, the more divergent behavior revealed by DMA reflects the more complex effect on mechanical properties.

AUTHOR CONTRIBUTIONS

Bettina Strommer: Conceptualization (lead); data curation (lead); investigation (lead); validation (lead); visualization (lead); writing – original draft (lead).

Dietmar Schulze: Formal analysis (supporting); methodology (supporting); writing – review and editing (supporting). **Bernhard Schartel:** Data curation (supporting); project administration (equal); supervision (equal); writing – original draft (supporting); writing – review and editing (equal). **Martin Böhning:** Conceptualization (supporting); methodology (supporting); supervision (lead); writing – original draft (equal); writing – review and editing (supporting).

ACKNOWLEDGMENTS

The authors thank Florian Engelmann for his help with the two-roll milling, hot-pressing, and sample preparation, Gauri Hasabnis for the micro-compounding, Leonardo Agudo-Jácome for the instructions on the TEM and Martina Bistriz for cryo-microtome cutting. Open Access funding enabled and organized by Projekt DEAL.

CONFLICT OF INTEREST STATEMENT


The authors declare no conflict of interest.

DATA AVAILABILITY STATEMENT

The data that support the findings of this study are available from the corresponding author upon reasonable request.

ORCID

Bettina Strommer  <https://orcid.org/0000-0002-2451-3287>

Bernhard Schartel  <https://orcid.org/0000-0001-5726-9754>

Martin Böhning  <https://orcid.org/0000-0001-9753-345X>

REFERENCES

- [1] S. Horikoshi, N. Serpone, in *Microwaves in Nanoparticle Synthesis* (Eds: S. Horikoshi, N. Serpone), Wiley-VCH, Weinheim **2013**, p. 1.
- [2] L. Bokobza, *Nanomaterials* **2019**, *9*, 1.
- [3] D. G. Papageorgiou, I. A. Kinloch, R. J. Young, *Carbon* **2015**, *95*, 460.
- [4] D. Z. Pirityi, T. Bárány, K. Pölöskei, *J. Appl. Polym. Sci.* **2022**, *139*, 32.
- [5] S. Cheng, X. Duan, Y. Cui, C. Liang, Z. Zhang, G. Zhao, Y. Liu, *J. Appl. Polym. Sci.* **2022**, *139*, 37.
- [6] Y. Wu, L. Chen, S. Qin, J. Li, H. Zhou, J. Chen, *J. Appl. Polym. Sci.* **2017**, *134*, 25.
- [7] B. Mensah, S. Kim, S. Arepalli, C. Nah, *J. Appl. Polym. Sci.* **2014**, *131*, 16.
- [8] D. Frasca, D. Schulze, V. Wachtendorf, C. Huth, B. Schartel, *Eur. Polym. J.* **2015**, *71*, 99.
- [9] M. Galimberti, V. Barbera, S. Guerra, A. Bernardi, *Rubber Chem. Technol.* **2017**, *90*, 2.
- [10] E. Kong, B. Yoon, J.-D. Nam, J. Suhr, *Macromol. Res.* **2018**, *26*, 11.
- [11] V. Kumar, U. Giese, T. Hanel, M. Galimberti, L. Giannini, *Kautschuk Gummi Kunststoffe* **2014**, *67*, 38.
- [12] C. F. Matos, F. Galembeck, A. J. G. Zarbin, *Carbon* **2014**, *78*, 469.
- [13] B. Mensah, K. C. Gupta, H. Kim, W. Wang, K. U. Jeong, C. Nah, *Polym. Test.* **2018**, *68*, 160.
- [14] B. Strommer, A. Battig, D. Frasca, D. Schulze, C. Huth, M. Böhning, B. Schartel, *ACS Appl. Polym. Mater.* **2022**, *4*, 2.
- [15] M. Tang, W. Xing, J. Wu, G. Huang, K. Xiang, L. Guo, G. Li, *J. Mater. Chem. A* **2015**, *3*, 11.
- [16] A. Battig, N. Fadul, D. Frasca, D. Schulze, B. Schartel, *E-Polymers* **2021**, *21*, 244.
- [17] D. Frasca, D. Schulze, M. Boehning, B. Krafft, B. Schartel, *Rubber Chem. Technol.* **2016**, *89*, 2.
- [18] D. Frasca, D. Schulze, V. Wachtendorf, B. Krafft, T. Rybak, B. Schartel, *Polymer* **2016**, *8*, 95. <https://doi.org/10.3390/polym8030095>
- [19] D. Frasca, D. Schulze, V. Wachtendorf, M. Morys, B. Schartel, *Polym. Adv. Technol.* **2016**, *27*, 7.
- [20] B. Zirnstein, W. Tabaka, D. Frasca, D. Schulze, B. Schartel, *Polym. Test.* **2018**, *66*, 268.
- [21] C. Nah, M. A. Kader, in *Rubber Nanocomposites: Preparation, Properties and Applications* (Eds: S. Thomas, R. Stephen), Singapore, John Wiley & Sons (Asia) Pte Ltd **2010**, p. 499.
- [22] J. Wang, K. Zhang, Q. Bu, M. Lavorgna, H. Xia, in *Carbon-related Materials in Recognition of Nobel Lectures by Prof. Akira Suzuki in ICCE* (Eds: S. Kaneko, P. Mele, T. Endo, T. Tsuchiya, K. Tanaka, M. Yoshimura, D. Hui), Springer, Cham **2017**, p. 175.
- [23] Y. H. Zhan, M. Lavorgna, G. Buonocore, H. S. Xia, *J. Mater. Chem.* **2012**, *22*, 21.
- [24] A. Hirsch, *Nat. Mater.* **2010**, *9*, 11.
- [25] S. Agnelli, S. Pandini, A. Serafini, S. Musto, M. Galimberti, *Macromolecules* **2016**, *49*, 22.
- [26] S. Agnelli, S. Pandini, F. Torricelli, P. Romele, A. Serafini, V. Barbera, M. Galimberti, *Express Polym. Lett.* **2018**, *12*, 8.
- [27] J. Dong, C. Wang, X. Fan, L. Wei, G. Shen, R. Sun, R. Li, *Nanomaterials* **2022**, *12*, 13.
- [28] M. Liu, S. Li, I. A. Kinloch, R. J. Young, D. G. Papageorgiou, *2D Materials* **2020**, *7*, 25031.
- [29] K. A. Mokhireva, A. L. Svistkov, V. V. Shadrin, *Proc. Struct. Integr.* **2021**, *32*, 137.
- [30] M. Galimberti, V. Kumar, M. Coombs, V. Cipolletti, S. Agnelli, S. Pandini, L. Conzatti, *Rubber Chem. Technol.* **2013**, *87*, 2.
- [31] Z. Li, R. J. Young, I. A. Kinloch, N. R. Wilson, A. J. Marsden, A. P. A. Raju, *Carbon* **2015**, *88*, 215.
- [32] Z. Li, R. J. Young, N. R. Wilson, I. A. Kinloch, C. Vallés, Z. Li, *Compos. Sci. Technol.* **2016**, *123*, 125.
- [33] D. R. Bortz, E. G. Heras, I. Martin-Gullon, *Macromolecules* **2012**, *45*, 1.
- [34] L. Gong, R. J. Young, I. A. Kinloch, I. Riaz, R. Jalil, K. S. Novoselov, *ACS Nano* **2012**, *6*, 3.
- [35] J. Liang, Y. Huang, L. Zhang, Y. Wang, Y. Ma, T. Guo, Y. Chen, *Adv. Funct. Mater.* **2009**, *19*, 14.
- [36] C. Vallés, I. A. Kinloch, R. J. Young, N. R. Wilson, J. P. Rourke, *Compos. Sci. Technol.* **2013**, *88*, 158.
- [37] R. J. Young, I. A. Kinloch, in *Nanoscience: Volume 1: Nanostructures Through Chemistry*, Vol. 1 (Ed: P. O'Brien), The Royal Society of Chemistry, Cambridge **2013**, p. 145.

- [38] S. Araby, Q. Meng, L. Zhang, H. Kang, P. Majewski, Y. Tang, J. Ma, *Polymer* **2014**, 55, 1.
- [39] A. Noël, J. Faucheu, J.-M. Chenal, E. Bourgeat-Lami, *Polymer* **2014**, 55, 20.
- [40] Y. Shi, W. Ma, L. Wu, D. Hu, J. Mo, B. Yang, S. Zhang, Z. Zhang, *J. Appl. Polym. Sci.* **2019**, 136, 37.
- [41] J. R. Potts, O. Shankar, L. Du, R. S. Ruoff, *Macromolecules* **2012**, 45, 15.
- [42] G. H. F. Bergmann, H. Finkelmann, V. Percec, M. Zhao, *Macromol. Rapid Commun.* **1997**, 18, 5.
- [43] J. Kuepfer, H. Finkelmann, *Macromol. Chem. Phys.* **1994**, 195, 1017.
- [44] H. Wermter, H. Finkelmann, *E-Polymers* **2001**, 1, 013. <https://doi.org/10.1515/epoly.2001.1.1.111>
- [45] B. Strommer, D. Schulze, B. Schartel, M. Böhning, *Polymer* **2022**, 14, 20.
- [46] A. R. Payne, *J. Appl. Polym. Sci.* **1965**, 9, 6.
- [47] P. J. Flory, J. J. Rehner, *J. Chem. Phys.* **1943**, 11, 11.
- [48] G. Kraus, *Rubber Chem. Technol.* **1957**, 30, 3.
- [49] G. Kraus, *J. Appl. Polym. Sci.* **1963**, 7, 3.
- [50] G. Kraus, *Angew. Makromol. Chem.* **1977**, 60, 1.

SUPPORTING INFORMATION

Additional supporting information can be found online in the Supporting Information section at the end of this article.

How to cite this article: B. Strommer, D. Schulze, B. Schartel, M. Böhning, *J. Appl. Polym. Sci.* **2023**, 140(16), e53753. <https://doi.org/10.1002/app.53753>